Enhanced Hybridization Sets the Stage for Electronic Nematicity in CeRhIn$_5$

P. F. S. Rosa,[1] S. M. Thomas,[1] F. F. Balakirev,[2] E. D. Bauer,[1] R. M. Fernandes,[3]
J. D. Thompson,[1] F. Ronning,[1] and M. Jaime[2]

[1]*Los Alamos National Laboratory, Los Alamos, New Mexico 87545, USA*
[2]*National High Magnetic Field Laboratory, Los Alamos, New Mexico 87545, USA*
[3]*School of Physics and Astronomy, University of Minnesota, Minneapolis, Minnesota 55455, USA*

High magnetic fields induce a pronounced in-plane electronic anisotropy in the tetragonal anti-ferromagnetic metal CeRhIn$_5$ at $H^* \gtrsim 30$ T for fields $\simeq 20°$ off the c axis. Here we investigate the response of the underlying crystal lattice in magnetic fields to 45 T via high-resolution dilatometry. At low fields, a finite magnetic field component in the tetragonal ab plane explicitly breaks the tetragonal (C_4) symmetry of the lattice revealing a finite nematic susceptibility. A modest a-axis expansion at H^* hence marks the crossover to a fluctuating nematic phase with large nematic susceptibility. Magneto-striction quantum oscillations confirm a Fermi surface change at H^* with the emergence of new orbits. By analyzing the field-induced change in the crystal-field ground state, we conclude that the in-plane Ce $4f$ hybridization is enhanced at H^*, in agreement with the in-plane lattice expansion. We argue that the nematic behavior observed in this prototypical heavy-fermion material is of electronic origin, and is driven by the hybridization between $4f$ and conduction electrons which carries the f-electron anisotropy to the Fermi surface.

For more than half a century, the investigation of rare-earth-based materials has provided predictive understanding in both fundamental and applied realms [1]. Cerium-based materials are a particularly intriguing case because their $4f$ electron may hybridize with the sea of conduction electrons [2]. The f-electron delocalization destabilizes the otherwise magnetically ordered ground state and novel phenomena may arise at the Fermi surface (FS). Heavy electron masses, unconventional superconductivity, and non-Fermi-liquid behavior are a few known examples of such emergent phenomena [3].

More recently, the discovery of a large electronic in-plane anisotropy induced by high magnetic fields in tetragonal CeRhIn$_5$ reveals the possibility of yet another state of matter, the so-called XY nematic [4]. In an electronic nematic phase, the symmetry of the electronic system is lowered compared to that of the underlying lattice, in analogy to the directional alignment in nematic liquid crystals without translational symmetry breaking [5,6]. Above an out-of-plane critical field of $H^* \approx 30$ T, but within the antiferromagnetic (AFM) phase, transport measurements reveal electronic nematicity in CeRhIn$_5$. The small in-plane field component necessary to break the rotational symmetry of the electronic structure suggests a remarkably large nematic susceptibility. Moreover, the modest magnetostriction anomaly at H^*, along with a similar response in the B_{1g} and B_{2g} channels, indicates that this phase is not strongly pinned to the lattice. At H^*, magnetization measurements also identify a FS

reconstruction with a larger FS in the nematic phase [7,8]. Possible scenarios, including correlated spin chains and two-dimensional frustrated magnetism due to competing exchange interactions, have been raised in the initial report [4], but a consensus on the origin of the nematic state remains to be reached.

At zero field and zero pressure, CeRhIn$_5$ undergoes a phase transition to a helix AFM order at $T_N = 3.8$ K with ordering wave vector $\mathbf{Q}_1 = (0.5, 0.5, 0.297)$ [9–11]. Pressurizing CeRhIn$_5$ tunes T_N toward a quantum-critical point (QCP) at $P_{c2} = 2.3$ GPa and induces unconventional superconductivity around it [12–14]. At P_{c2} the effective electron mass diverges and the FS changes abruptly [15]. Applied pressure is a clean tuning parameter known to increase the $4f$ hybridization, and therefore the T-P phase diagram of CeRhIn$_5$ can be qualitatively understood in terms of the strength of the (Kondo) coupling between $4f$ and conduction electrons [16]. Remarkably, magnetic fields also tune T_N towards a QCP at ≈ 50 T and a FS reconstruction is observed at $H^* \approx 30$ T [7]. Magnetic fields, however, are symmetry breaking and expected to localize $4f$ electrons. Understanding why the Kondo coupling is robust in high fields is a first step towards unveiling the nature of the nematic phase. An additional relevant question is whether the H^* boundary is a true (first-order) phase transition or a crossover.

To answer these questions, probes other than electrical resistivity are imperative. Thermodynamic probes such as torque magnetometry, magnetic susceptibility, and specific

heat, however, fail to observe an anomaly at H^*, although their response changes above it [17]. In this Letter, we use high-resolution dilatometry to probe the response of the underlying lattice to magnetic fields. The finite coupling between the nematic phase and the lattice yields an anomaly at H^* that vanishes above the AFM boundary. An in-plane field component explicitly breaks the tetragonal (C_4) symmetry of the lattice revealing a finite nematic susceptibility at low fields. A modest a-axis expansion at $H^* = 31$ T hence marks the crossover to a fluctuating nematic phase with large nematic susceptibility. This crossover occurs concomitantly to a FS change at H^* and an enhancement in the Ce $4f$ hybridization, suggesting that the nematic phase stems from the $4f$ degrees of freedom (d.o.f.) and their anisotropy, which is translated to the FS via hybridization. The FS change is confirmed by unprecedented quantum oscillations in the magnetostriction of CeRhIn$_5$.

The first point we will address is how the system responds to an in-plane field that explicitly breaks C_4 symmetry. Figure 1 shows the anisotropic magnetostriction of CeRhIn$_5$ obtained with a capacitance dilatometer with fields along the a axis. When $dL||H||a$, the longitudinal magnetostriction is negative and displays a sharp contraction at 2.2 T, signaling the transition from a helix state (AF1) to a commensurate collinear square-wave state (AF3) with ordering vector $\mathbf{Q}_3 = (1/2, 1/2, 1/4)$ [11]. The transverse magnetostriction ($dL||b$), however, is positive and displays a sharp expansion at 2.2 T. In a conventional material, compression along one axis produces an expansion along the perpendicular axes, and the ratio of the perpendicular strains is known as the Poisson's ratio, ν_{ij} [18]. In particular, ν_{xy} gives the in-plane strain response. The calculated Poisson's ratio of CeRhIn$_5$ is $\nu_{xy} \equiv s_{xy}/s_{xx} = 0.2$, where s_{ij} are the elastic compliances obtained from the inverted elastic modulus tensor [19]. The in-plane experimental ratio, however, is not only 2–3 times larger than the calculated one, but also field and temperature dependent. This disagreement suggests that there are other d.o.f. contributing to the observed response.

To describe these observations and model the magnetoelastic coupling, we write the magnetoelastic free energy of a tetragonal system as $-\lambda\delta(H_a^2 - H_b^2) + (\alpha/2)\delta^2$ to ensure time-reversal symmetry. Here $\delta = (a - b)/a$ is the orthorhombic distortion, λ is a coupling constant, and α is the elastic constant renormalized by nematic fluctuations acting as an indirect measure of the nematic susceptibility. As a result, one can estimate the nematic susceptibility, χ_{nem}, from the data via $\chi_{nem} \propto \partial\delta/\partial H_a^2$, where $\delta = dL_a/L_a - dL_b/L_b$. Our fits show that $\gamma\chi_{nem} = -2 \times 10^{-9}$ in the AF1 phase and $\gamma\chi_{nem} = -6 \times 10^{-10}$ in the AF3 phase, where γ is a coupling constant. The nematic susceptibility is finite, but curiously smaller in AF3, indicating that χ_{nem} is not enhanced as a function of magnetic fields at low fields.
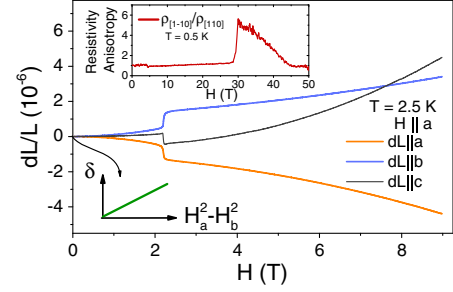

FIG. 1. Magnetostriction of CeRhIn$_5$ along the a axis, dL_a/L_a, at 2.5 K for fields applied in the tetragonal ab plane. Top inset shows the in-plane anisotropy in electrical resistivity [4]. Bottom inset shows a schematic diagram of the order parameter δ as a function of the in-plane symmetry breaking field indicating that there is no intercept when the in-plane field goes to zero (see also Supplemental Material [20]).

In fact, the nematic response in the electronic d.o.f., i.e., in-plane resistivity anisotropy, is vanishingly small at low fields and increases sharply at H^* (inset of Fig. 1). We note that the nematic order parameter couples to any quantity that breaks tetragonal symmetry. Therefore, nematic fluctuations—and hence the corresponding χ_{nem}—can be indirectly probed in different quantities, such as the elastic constant α or the rate of change of the anisotropic resistivity, with different coupling strengths.

Next, we turn our attention to the lattice response at fields applied $20°$ off the c axis at which the in-plane resistivity anisotropy is pronounced. Figure 2 shows the anisotropic magnetostriction of CeRhIn$_5$ obtained via optical dilatometry. A reference optical sensor in the same optical fiber is measured simultaneously to ensure that the fiber response is field independent and negligible compared to the response of CeRhIn$_5$. At low fields, a broad feature is observed at $H_{MM} \sim 7.6$ T reminiscent of the AF1-AF3 transition discussed above. Applying the known $1/\sin(\theta)$ dependence of this transition, we obtain that the actual angle between the c axis and the applied field is $\theta = 17°$. At higher fields, an anomaly is buried in the background and the insets of Fig. 2 show the magnetostriction after the subtraction of a 4th order polynomial fit obtained in the range $15 < H < 29$ T. The subtracted data show a small lattice expansion at 31 T along the a axis, $dL_a/L_a = +1.3 \times 10^{-6}$, whereas a small lattice contraction occurs along the c axis, $dL_c/L_c = -1.8 \times 10^{-6}$, in agreement with the upper limit of -2×10^{-6} obtained recently in pulsed fields [4].

Remarkably, there is no noticeable hysteresis in our data, in contrast with the hysteretic resistivity obtained in thin microstructured samples, but in agreement with virtually hysteresis-free resistivity curves obtained in larger samples [23]. The lack of hysteresis along with a broader transition in bulk samples suggests that H^* might actually be a crossover to a regime with large nematic susceptibility, which in turn is highly sensitive to strain. As elaborated in
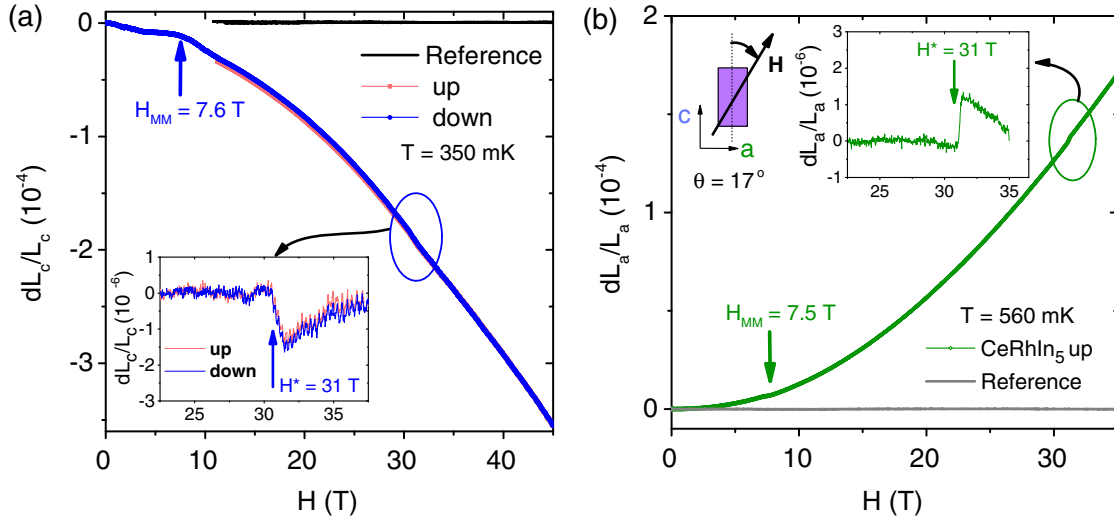
FIG. 2. Magnetostriction of CeRhIn$_5$ along (a) the c axis at $T = 350$ mK and (b) the a axis at $T = 560$ mK for fields applied $\simeq 20°$ off the c axis. Here θ is the polar angle between the applied field and the c axis. The azimuthal angle is set to $\phi = 90°$. Insets show the data after a background subtraction.

Ref. [23], microstructured samples are coupled to the substrate, and the strain relaxation might be different in thinner samples. As a result, smaller samples may take longer to relax to equilibrium and hence may display hysteresis.

The inset of Fig. 2(a) also shows sizable quantum oscillations at $H \gtrsim 27$ T. Although quantum oscillations (QO) in magnetostriction is a phenomenon known since the 1960s [24], this is the first time magnetostriction QO are reported in CeRhIn$_5$, likely due to the fact that high-quality single crystals, high-resolution dilatometers, and low-noise environments (i.e., dc fields) are required. The amplitude of oscillations along the c axis can be written as $-MH(\partial \ln A / \partial \sigma_c)$, where M is the amplitude of oscillations in magnetization, A is the extremal cross-sectional area of the FS perpendicular to the applied magnetic field, and σ_c is the stress along the c axis. Magnetostriction QO thus provide information on the FS of materials, as do magnetization QO (i.e., dHvA), but the additional term $\partial \ln A / \partial \sigma_c$ enhances the amplitude of the stress-sensitive orbits.

Figure 3(a) shows the magnetostriction QO in inverse field and Fig. 3(b) shows the corresponding FFT spectra. We observe four frequencies which agree well with the frequencies obtained via dHvA for $30 < H < 45$ T at 330 mK and fields along the c axis ($\alpha_3 = 3.7$, $\alpha'_2 = 5$, $\alpha'_1 = 5.7$, and $\beta_2 = 6.3$ kT) [8]. We note that dHvA frequencies α'_2 and α'_1 are observed only above H^*. By comparing the amplitude of the orbits given by the different techniques in similar conditions, one can obtain information on the strain dependence of the orbits. For instance, the β_2 amplitude is reduced in our data as compared to dHvA results whereas the α'_2 is relatively enhanced. These results suggest that α'_2 orbit is a more strain-sensitive orbit than β_2.

Figure 4(a) shows the c-axis magnetostriction at various temperatures for fields applied $\simeq 20°$ off the c axis. As T increases, H^* remains fairly constant, but deviates to slightly lower fields before vanishing above T_N. We note that the anomaly at H^* detected in transport measurements becomes unobservable at $T > 2.2$ K, which could be a consequence of resolution limitations. By tracking H^* to higher temperatures, we are able to affirm that the nematic boundary most likely intercepts the AFM boundary and disappears above T_N, as shown in the $H - T$ phase diagram to be discussed below (Fig. 5).

Figure 4(b) shows the high-field quantum oscillations in magnetostriction with increasing temperature. Although we are unable to reliably extract the T dependence of the orbits α'_2, α'_1, and β_2 due to their small amplitudes, α_3 is significantly more intense and can be tracked to higher
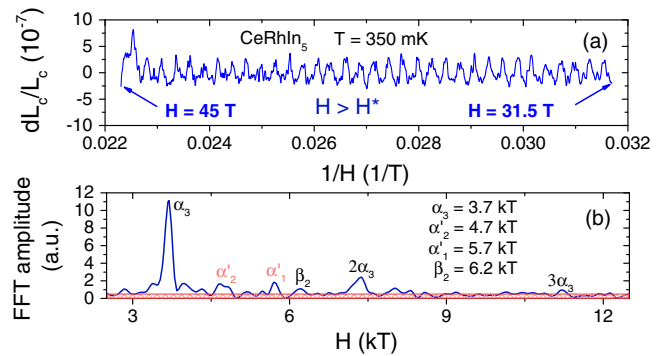

FIG. 3. (a) Magnetostriction of CeRhIn$_5$ at 350 mK as a function of inverse field for fields applied $\simeq 20°$ off the c axis. A high-pass filter was used to remove low-frequency oscillations that likely originate from the background difference below and above H^*. (b) FFT spectra in the region $31.5 < H < 45$ T. The dashed area is an estimate of the noise floor.
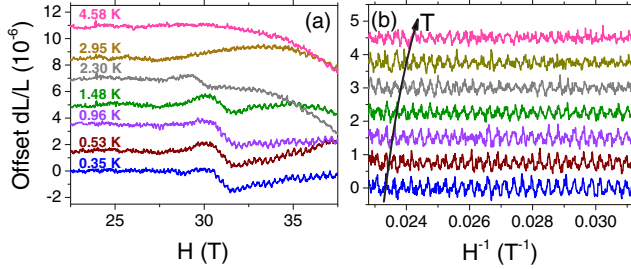
FIG. 4. (a) Temperature dependence of the magnetostriction of CeRhIn$_5$ for fields applied $\simeq 20°$ off the c axis. An offset is added for clarity. (b) High-field quantum oscillations in inverse field obtained from the data shown in panel (a). The color scheme is the same in both panels.

temperatures. Remarkably, the overall amplitude of the oscillations does not display the expected behavior for conventional metals within the Lifschitz-Kosevich (LK) formalism. According to the LK formula, the amplitude of the oscillations in a particular field range increases with decreasing temperature as $\propto m^*T/\sinh(Cm^*T)$, where C is a constant and m^* the effective mass [25]. Although the amplitude of the oscillations do decrease when comparing the temperature extremes (4.58 and 0.35 K), there is no clear trend below 1 K. This is in agreement with dHvA measurements, both in pulsed and dc fields, that observe a decrease in the amplitude of the α_3 orbit below about 1 K [17,26]. The interpretation of this anomalous behavior, however, is not settled. On one hand, the early report in pulsed fields attributes this decrease to the formation of spin-density-wave order [26]. On the other hand, more recent dHvA results in dc fields support a spin-dependent mass enhancement of the FS. In the latter, the QO amplitude is well described by a spin-dependent LK formula, suggesting a spin-split FS, as observed previously in CeCoIn$_5$ [17,27]. In fact, we observe a beating pattern at frequencies close to α_3, which could be taken as indicative of two Fermi pockets close together, one spin-up and one spin-down.

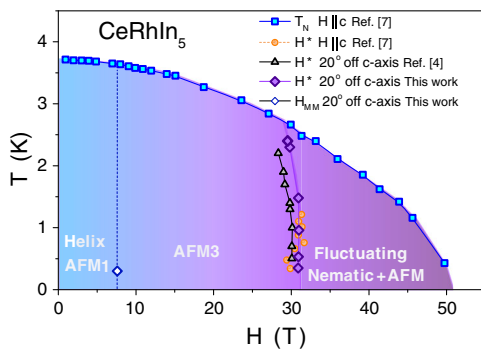Finally, we discuss the implications of our results for the nature of the nematic phase. Figure 5 displays the H-T

FIG. 5. H-T phase diagram of CeRhIn$_5$. Data from Ref. [7] were obtained by specific heat and Hall measurements. Data from Ref. [4] were obtained by electrical resistivity.

phase diagram of CeRhIn$_5$ with a compilation of recent high-field data. Because this phase diagram is constructed in the presence of a tetragonal symmetry-breaking in-plane magnetic field, the phase boundary at H^* should be understood as a crossover, instead of a true nematic phase transition. In fact, removing the magnetic field does not seem to result in a residual hysteretic resistivity anisotropy [4], which is indicative of a large nematic susceptibility, but no long-range nematic order. We cannot, however, rule out that another symmetry of the system may be broken at H^* and a true phase transition occurs due to other d.o.f.

If not long-range nematic order, what changes at H^* that causes a large nematic susceptibility and why is the Kondo coupling robust in high magnetic fields? We recall that recent dHvA measurements reveal a FS change at H^* pointing to a larger FS in the nematic phase [7]. This indicates that the $4f$ electrons are becoming more itinerant as they are incorporated to the FS at H^*. Therefore, the main tuning parameter here must be the strength of the $4f$-conduction electron hybridization. The key point is that the hybridization depends on the Ce $4f$ ground-state wave function, which is given by the crystal-field parameters in this particular tetragonal structure. Thus, the answer to our question lies in the field dependence of the wave functions determined by the crystalline electric field (CEF) and their anisotropic hybridization. For CeRhIn$_5$, the low-energy CEF levels are given by [28]

$$|0\rangle = \Gamma_7^2 = \alpha|\pm 5/2\rangle - \beta|\mp 3/2\rangle, \quad \alpha = 0.62,$$
$$|1\rangle = \Gamma_7^1 = \beta|\pm 5/2\rangle + \alpha|\mp 3/2\rangle, \quad \beta = 0.78, \qquad (1)$$

where $|0\rangle$ is the ground state, $|1\rangle$ is the first-excited state at 7 meV, and α^2 determines the out-of-plane anisotropy. The pure $|5/2\rangle$ orbital is donut shaped and hence higher α^2 corresponds to a more oblate $4f$ orbital confined to the ab plane. Linear-polarized x-ray absorption experiments reveal that the ground-state doublet changes from flatter (i.e., larger $|5/2\rangle$) orbitals in CeRhIn$_5$ to orbitals that are more extended along the c axis in CeIrIn$_5$ and CeCoIn$_5$ (i.e., smaller $|5/2\rangle$) [29]. The prolate orbitals hybridize more strongly with out-of-plane In(2) electrons and yield superconducting ground states in CeIrIn$_5$ and CeCoIn$_5$.

Now we turn our attention to the field dependence of the orbitals in Eq. (1). Magnetic fields will, by the Zeeman effect, split the Γ_7 doublets and, therefore, promote mixing between the ground state and the first-excited state. Interestingly, the $|5/2\rangle$ contribution in the first excited state ($\beta = 0.78$) is larger than that of the original ground state ($\alpha = 0.62$), implying that the new, field-induced ground state wave function will become more confined to the basal plane. Because of its modified shape, the new ground state displays an enhanced hybridization with the in-plane In(1) electrons, similar to what happens with Sn-doped CeMIn$_5$ ($M = $ Co, Rh) [30]. We note that this hybridization increase with In(1) electrons may be fundamentally different from the

hybridization with In(2) electrons observed in $CeIrIn_5$, $CeCoIn_5$, and likely $CeRhIn_5$ under pressure [31]. This scenario explains not only why the FS increases at H^* with the field-induced incorporation of $4f$ electrons, but it may also be the reason $CeRhIn_5$ is not superconducting as a function of field or Sn doping. Importantly, a similar crystal-field scenario has been used to explain recent nuclear magnetic resonance experiments in high fields [32]. The fact that H^* exists only inside the AFM state along with the correlation between enhanced hybridization and enhanced nematic susceptibility suggests that the nematic phase stems from the f-electron d.o.f. Whether these are a consequence of the frustration and the field-induced magnetic anisotropy in the spin d.o.f. known to exist in $CeRhIn_5$ [11,33] or a consequence of the hybridization gap itself remains an open question.

In summary, we performed high-resolution magnetostriction measurements in $CeRhIn_5$ in dc fields to 45 T. At low fields, a finite in-plane field explicitly breaks the tetragonal (C_4) symmetry of the underlying lattice and reveals a finite nematic susceptibility. At high fields, a small expansion in the a-axis magnetostriction marks the onset of the nematic response at $H^* = 31$ T for fields $\simeq 20°$ off the c axis. The H-T phase diagram hence hosts a crossover line at H^* to a fluctuating nematic phase with high nematic susceptibility. This crossover occurs concomitantly to an enhancement in the Ce $4f$ hybridization with the in-plane In(1) conduction electrons, which explains why the Kondo coupling is robust in high fields. Our results suggest that the nematic phase stems from the $4f$ d.o.f. and their anisotropy translated to the Fermi surface via hybridization. As a consequence, we argue that the nematic behavior observed here in a prototypical heavy-fermion material is of electronic origin, and is driven by hybridization.

[1] J. Jensen and A. R. Mackintosh, *Rare Earth Magnetism* (Clarendon Press, Oxford, 1991).

[2] P. Coleman, *Heavy Fermions: Electrons at the Edge of Magnetism*, Handbook of Magnetism and Advanced Magnetic Materials (John Wiley & Sons, New York, 2007).

[3] H von Lohneysen, A. Rosch, M. Votja, and P. Wolfle, Rev. Mod. Phys. **79**, 1015 (2007).

[4] F. Ronning, T. Helm, K. R. Shirer, M. D. Bachmann, L. Balicas, M. K. Chan, B. J. Ramshaw, R. D. McDonald, F. F. Balakirev, M. Jaime, E. D. Bauer, and P. J. W. Moll, Nature (London) **548**, 313 (2017).

[5] E. Fradkin, S. A. Kivelson, M. J. Lawler, J. P. Eisenstein, and A. P. Mackenzie, Annu. Rev. Condens. Matter Phys. **1**, 153 (2010).

[6] R. M. Fernandes, A. V. Chubukov, and J. Schmalian, Nat. Phys. **10**, 97 (2014).

[7] L. Jiao, Y. Chen, Y. Kohama, D. Graf, E. D. Bauer, J. Singleton, Jian-Xin Zhu, Z. Weng, G. Pang, T. Shang, J. Zhang, Han-Oh Lee, T. Park, M. Jaime, J. D. Thompson, F. Steglich, Q. Si, and H. Q. Yuan, Proc. Natl. Acad. Sci. U.S.A. **112**, 673 (2015).

[8] L. Jiao, Z. F. Weng, M. Smidman, D. Graf, J. Singleton, E. D. Bauer, J. D. Thompson, and H. Q. Yuan, Philos. Mag. **97**, 3446 (2017).

[9] W. Bao, P. G. Pagliuso, J. L. Sarrao, J. D. Thompson, Z. Fisk, J. W. Lynn, and R. W. Erwin, Phys. Rev. B **62**, R14621 (R) (2000).

[10] D. M. Fobes, E. D. Bauer, J. D. Thompson, A. Sazonov, V. Hutanu, S. Zhang, F. Ronning, and M. Janoschek, J. Phys. Condens. Matter **29**, 17LT01 (2017).

[11] D. M. Fobes, S. Zhang, S.-Z. Lin, P. Das, N. J. Ghimire, E. D. Bauer, J. D. Thomson, L. W. Harriger, G. Ehlers, A. Podlesnyak, R. I. Bewley, A. Sazonov, V. Hutanu, F. Ronning, C. D. Batista, and M. Janoschek, Nat. Phys. **14**, 456 (2018).

[12] H. Hegger, C. Petrovic, E. G. Moshopoulou, M. F. Hundley, J. L. Sarrao, Z. Fisk, and J. D. Thompson, Phys. Rev. Lett. **84**, 4986 (2000).

[13] T. Park, F. Ronning, H. Q. Yuan, M. B. Salamon, R. Movshovich, J. L. Sarrao, and J. D. Thompson, Nature (London) **440**, 65 (2006).

[14] T. Mito, S. Kawasaki, Y. Kawasaki, G.-q. Zheng, Y. Kitaoka, D. Aoki, Y. Haga, and Y. Onuki, Phys. Rev. Lett. **90**, 077004 (2003).

[15] H. Shishido *et al.*, J. Phys. Soc. Jpn. **71**, 162 (2002).

[16] L. Mendonça-Fereira *et al.*, Phys. Rev. Lett. **101**, 017005 (2008).

[17] L. Jiao, M. Smidman, Y. Kohama, Z. S. Wang, D. Graf, Z. F. Weng, Y. J. Zhang, A. Matsuo, E. D. Bauer, Hanoh Lee, S. Kirchner, J. Singleton, K. Kindo, J. Wosnitza, F. Steglich, J. D. Thompson, and H. Q. Yuan, arXiv:1711.06191.

[18] A. Ballato, IEEE Trans. Ultrason. Ferroelectr. Freq. Control **43**, 56 (1995).

[19] R. S. Kumar, H. Kohlmann, B. E. Light, A. L. Cornelius, V. Raghavan, T. W. Darling, and J. L. Sarrao, Phys. Rev. B **69**, 014515 (2004).

[20] See Supplemental Material at http://link.aps.org/supplemental/10.1103/PhysRevLett.122.016402, which includes Refs. [21,22].

[21] G. M. Schmiedeshoff, A. W. Lounsbury, D. J. Luna, S. J. Tracy, A. J. Schramm, S. W. Tozer, V. F. Correa, S. T. Hannahs, T. P. Murphy, and E. C. Palm, Rev. Sci. Instrum. **77**, 123907 (2006).

[22] M. Jaime *et al.*, Sensors **17**, 2572 (2017).

[23] P. J. W. Moll, B. Zeng, L. Balicas, S. Galeski, F. F. Balakirev, E. D. Bauer, and F. Ronning, Nat. Commun. **6**, 6663 (2015).

[24] B. A. Green, Jr. and B. S. Chandrasekhar, Phys. Rev. Lett. **11**, 331 (1963).

[25] D. Shoenberg, *Magnetic Oscillations in Metals* (Cambridge University Press, Cambridge, England, 1984).

[26] A. L. Cornelius, A. J. Arko, J. L. Sarrao, M. F. Hundley, and Z. Fisk, Phys. Rev. B **62**, 14181 (2000).

[27] A. McCollam, S. R. Julian, P. M. C. Rourke, D. Aoki, and J. Flouquet, Phys. Rev. Lett. **94**, 186401 (2005).

[28] T. Willers *et al.*, Phys. Rev. B **81**, 195114 (2010).

[29] T. Willers *et al.*, Proc. Natl. Acad. Sci. U.S.A. **112**, 2384 (2015).

[30] K. Chen, F. Strigari, M. Sundermann, Z. Hu, Z. Fisk, E. D. Bauer, P. F. S. Rosa, J. L. Sarrao, J. D. Thompson, J. Herrero-Martin, E. Pellegrin, D. Betto, K. Kummer, A. Tanaka, S. Wirth, and A. Severing, Phys. Rev. B **97**, 045134 (2018).

[31] J. H. Shim, K. Haule, and G. Kotliar, Science **318**, 1615 (2007).

[32] G. G. Lesseux *et al.*, *Proceedings of the SCES Meeting, Prague* (2017).

[33] P. Das, S.-Z. Lin, N. J. Ghimire, K. Huang, F. Ronning, E. D. Bauer, J. D. Thompson, C. D. Batista, G. Ehlers, and M. Janoschek, Phys. Rev. Lett. **113**, 246403 (2014).